AGU PUBLICATIONS

Water Resources Research

RESEARCH ARTICLE
10.1002/2016WR019182

Using web-based observations to identify thresholds of a person's stability in a flow

L. Milanesi[1], M. Pilotti[1], and B. Bacchi[1]

[1]Department of Civil, Environmental, Architectural Engineering and Mathematics, Università degli Studi di Brescia, Brescia, Italy

Key Points:
- A citizen science-based approach to assess human stability in a flow from online resources is proposed
- A data set of observations from real events is provided
- A probabilistic approach to identify thresholds of a person's vulnerability in a flow is proposed

Supporting Information:
- Supporting Information S1
- Data Set S1

Correspondence to:
L. Milanesi,
luca.milanesi@unibs.it

Citation:
Milanesi, L., M. Pilotti, and B. Bacchi (2016), Using web-based observations to identify thresholds of a person's stability in a flow, *Water Resour. Res.*, *52*, doi:10.1002/2016WR019182.

Received 9 MAY 2016
Accepted 17 SEP 2016
Accepted article online 26 SEP 2016

Abstract Flood risk assessment and mitigation are important tasks that should take advantage of rational vulnerability models to increase their effectiveness. These models are usually identified through a relevant set of laboratory experiments. However, there is growing evidence that these tests are not fully representative of the variety of conditions that characterize real flood hazard situations. This paper suggests a citizen science-based and innovative approach to obtain information from web resources for the calibration of people's vulnerability models. A comprehensive study employing commonly used web engines allowed the collection of a wide set of documents showing real risk situations for people impacted by floods, classified according to the stability of the involved subjects. A procedure to extrapolate the flow depth and velocity from the video frames is developed and its reliability is verified by comparing the results with observation. The procedure is based on the statistical distribution of the population height employing a direct uncertainty propagation method. The results complement the experimental literature data and conceptual models. The growing availability of online information will progressively increase the sample size on which the procedure is based and will eventually lead to the identification of a probability surface describing the transition between stability and instability conditions of individuals in a flow.

1. Introduction

Several factors contribute to make floods the World's most devastating and costly hazard: growing population, increasing inhabitant density in flood-prone areas at the global scale [e.g., *Güneralp et al.*, 2015; *Muis et al.*, 2015] with the inevitable increase of exposure, and hydrological cycle intensification triggered by climate change [e.g., *Min et al.*, 2011]. This is especially true for less developed countries since several national and regional studies in Europe [e.g., *Barredo*, 2009; *Jongman et al.*, 2014; *Fuchs et al.*, 2015] show more complex spatial and temporal trends of exposure and flood losses due to the effects of protection measures. Considering that structural risk mitigation measures are often unfeasible, nonstructural protection measures are becoming a priority with strong economic implications. For instance, the European Flood directive 2007/60/CE enforced these activities among European Union members. Therefore, rational approaches are needed to assess and comprehensibly model the risk components. While the computation of hazard intensity is usually accomplished with sophisticated numerical methods for the solution of the Shallow Water Equations [e.g., *Costabile et al.*, 2016; *Pilotti et al.*, 2010, 2011, 2014], the computation of vulnerability is a relatively younger issue. Several relevant contributions are available in the field of people's and buildings vulnerability [e.g., *Merz et al.*, 2010; *Pilotti et al.*, 2016; *Totschnig and Fuchs*, 2013] but in general a technical gap still exists in this field and the applications of such models in practice needs a process of critical homogenization. In this direction, this paper focuses on people's vulnerability to floods that claimed more than 55,000 fatalities in the period between 2001 and 2011, often related to unawareness and erroneous risk perception [e.g., *Becker et al.*, 2015].

Several experimental investigations in controlled conditions [*Foster and Cox*, 1973; *Abt et al.*, 1989; *Takahashi et al.*, 1992; *Karvonen et al.*, 2000; *Yee*, 2003; *Jonkman and Penning-Rowsell*, 2008; *Russo et al.*, 2013; *Martínez-Gomariz et al.*, 2016] explored the stability of individuals in flumes or real channels, by measuring the limiting flow depth h and velocity U that allow individuals to maintain control of their position. Complex experimental apparatus and safety equipment are required to test a wide range of flow depths and velocities. For

© 2016. American Geophysical Union. All Rights Reserved.

this reason, some recent experimental studies were conducted on scaled models, exploring the stability of people impacted by steady flows [*Xia et al*., 2014] or tidal bores [*Pan and Chanson*, 2015].

On the other hand, conceptual schemes mechanically explain the role of flow velocity and depth on the stability of a simplified geometry of the impacted body but require empirical stability observations for their calibration. *Love* [1987] first investigated the failure mechanisms of a rectangular monolith introducing the effect of the buoyancy force on both slipping and toppling instability mechanisms. This study prompted the development of several models that progressively improved the geometry of the body, the acting forces, and the failure mechanisms [*Keller and Mitsch*, 1993; *Lind et al*., 2004; *Walder et al*., 2006; *Ishigaki et al*., 2008; *Jonkman and Penning-Rowsell*, 2008; *Xia et al*., 2014]. Finally, *Milanesi et al*. [2015] reduced the number of experimental parameters and suggested a conceptual scheme to account also for the role of local ground slope and fluid density, providing a best fit to the available experimental data.

Up to now, the experimental data set available in the literature is made up of about 150 (U,h) threshold values for adults and 30 points for children. It is interesting to observe that this data set shows a remarkable variability [e.g., *Cox et al*., 2010] depending on test conditions (e.g., ground friction, slope, movement, and lighting), the physical features of the subjects, their equipment, and the assumed definition of instability. Accordingly, for a fixed flow depth, significant differences between the limiting velocities can be observed. For instance, *Abt et al*. [1989] recorded up to 15 different threshold velocities for human stability in the range between 1.25 and 3 m s^{-1} corresponding to a flow depth of about 0.75 m. The scattering of the experimental results emphasizes their intrinsic subjective dependence that physically based models partially explain only through different body parameters. However, a sensitivity analysis on the parameters of the same physical models shows that the incidence of psychological attitudes must be even more relevant. In real situations, environmental conditions and other secondary elements (e.g., lighting, debris, backpacks, and water temperature) will certainly inflate this spread. Accordingly, for practical application, a single stability threshold is not fully satisfying and a representative curve should be based on a large set of situations. In addition, as observed by *Abt et al*. [1989], the results obtained under controlled laboratory conditions are beset by some fundamental biases: subjects showed greater confidence due to the presence of safety equipment, soon became experienced and learned how to adjust to the flow, shed additional loads, and favored well-illuminated environments [see also *Russo et al*., 2013; *Martínez-Gomariz et al*., 2016]. On the contrary, *Karvonen et al*. [2000] suggested that the presence of survival suits in the RESCDAM tests could increase buoyancy and the hydrodynamic action. Moreover, the subjects were usually selected for good physical condition and an ideal age range. *Chanson and Brown* [2015] experienced firsthand the effects of turbid highly turbulent flows during the 2011 Brisbane River flood when both the presence of underwater obstacles and the impossibility to see ideal foot placement increased the risk level and the subject's insecurity feeling (H. Chanson, personal communication, 2016). These observations suggest that the traditional laboratory approach does not necessarily yield the most representative results. Also, the tests for the scaled models are not entirely satisfactory since a dummy cannot adjust its posture with respect to the flow and is not affected by psychological factors that influence stability under real conditions. Accordingly, the issue of data representativeness and realism must be addressed.

An important contribution to overcome these drawbacks could come by visual information available in the World Wide Web. A large amount of video footage documents the real interaction of people with floods and waves in many extreme situations that could not be reproduced in any laboratory experiment. Due to the increasing availability of reporting instruments and sharing platforms, this set of videos keeps increasing in number and quality [e.g., *Peduzzi et al*., 2012]. This paper shows how to obtain information on the stability of human beings impacted by flows from these footages. Moreover, it provides an example of what *Montanari et al*. [2013] envisaged in their visionary Editorial on the future challenges of research in the field of water resources. In other words, this study provides a practical application of technical and scientific exploitation of new observational systems that goes beyond classical data collection and includes citizen science. We propose to overcome experimental limitations, by widening "the spectrum of what and how we can observe, seeking an innovative effort to profit from the availability of an ever increasing flow of information" [*Montanari et al*., 2013].

This study took advantage of the videos recorded by untrained citizens published on the internet. Research projects involving nonprofessionals are well established in the field of environmental sciences [e.g., *Cohn*, 2008; *Dickinson et al*., 2012] and are growing also in the field of water resources [e.g., *Buytaert et al*., 2016].

Involvement by lawpersons was reported from studies concerning the definition of guidelines for flood map design [e.g., *Meyer et al*., 2012] and data assimilation in hydrological modeling [e.g., *Mazzoleni et al*., 2015]. The participation of the general public in research activities increases the availability of data that could not be collected otherwise or so economically. In this research, the footages were initially classed on the basis of their overall quality and only the videos that could provide reliable information were selected. A set of procedures to extrapolate quantitative information from the footages was proposed. Finally, the nature of the resulting data set suggests casting the problem of an individual's stability in a statistical framework, in place of a deterministic identification of a limiting curve, as done so far in the literature. Accordingly, a methodology to identify the stability surface in terms of probability and obtain a reference threshold is proposed. In our opinion, the informative content that can be retrieved with the procedures outlined in this paper will be progressively refined by the increase of available documents and will asymptotically converge to the "real" average threshold of an individual's stability in a flow.

2. Materials

Extensive research was carried out on the most common web search engines (e.g., Google.com) and broadcasting web sites (e.g., Youtube.com) to find videos of water-related accidents involving people. *Maurais* [2003] showed that web pages written in English, Italian, French, Spanish, Portuguese, Hindi, Chinese, Russian, and Arab amount to 83% of the total. Accordingly, keywords related to both floods and waves and their effects on people were selected and searched in these languages. Single images were not usually considered because of the impossibility to observe the movements of the person, to evaluate their stability, and the overall dynamics of the process.

The search of videos involving people impacted by a flow was also guided by the geographic distribution of flood events. The global flood inventory (GFI) [*Adhikari et al*., 2010] of events recorded from 1998 to 2008 shows the worldwide distribution of flood-prone areas and their main meteorological forcing functions, such as continental rainfalls (northeast U.S., Europe, and China), monsoons (India and Southeast Asia), and land falling tropical cyclones (Asia, Caribbean, and central America). According to *Kundzewicz et al*. [2014], most of the destructive flood events are concentrated in India, China and Bangladesh, where 75% of the fatalities recorded in the GFI occurred. Moreover, the same Authors show more events and fatalities occur in the Northern Hemisphere (where around 88–90% of the earth's total population lives) compared to the Southern Hemisphere, in ratio 19:1 and 4:1, respectively. These figures reflect the violence of the events and the presence of structural and nonstructural flood protection measures.

The availability of flood-related videos is also strongly influenced by the diffusion of technology and internet access. Accordingly, it is possible that the most flood-prone areas are not the best documented ones as demonstrated by the fact that a high proportion of the retrieved footages are from the Americas (Figure 1b). From 2009, there is a linear temporal increase of the number of available documents (Figure 1a) with a rate that would double the current data set by 2025.

In the selection of the videos, the issues of authenticity, quality, and type of recorded event must be addressed. In order to reject potentially manipulated videos, a general assessment of the flow pattern as well as of the reactions and the movements of the involved people was performed taking into account the possible comments posted by the users. As far as quality is concerned, the most common difficulties were related to low-resolution images (e.g., Figure 2a). In other situations, the calculation of lengths was affected by the zenithal shooting angle that strongly distorted the perspective (Figure 2b). Finally, an individual's stability is usually studied under the assumption of steady flow within gradually varied currents. Accordingly, this approach seems inappropriate for wave-related events when the wave front has a shock-like nature. In such situations, experimental and theoretical studies showed that the dynamic action exerted on the obstacle is amplified with respect to a steady state situation [e.g., *Aureli et al*., 2015; *Cross*, 1967]. For this reason, the videos with waves breaking directly on the person were discarded. However, several observations suggested that if the wave grows gradually, the person does not fall due to the impact with the wave front but when the body is already submerged in an apparently gradually varied flow. Accordingly, the selected set of footages does not include cases with significant sediment transport and includes only nine wave-related videos where flow behaved in a gradual fashion.

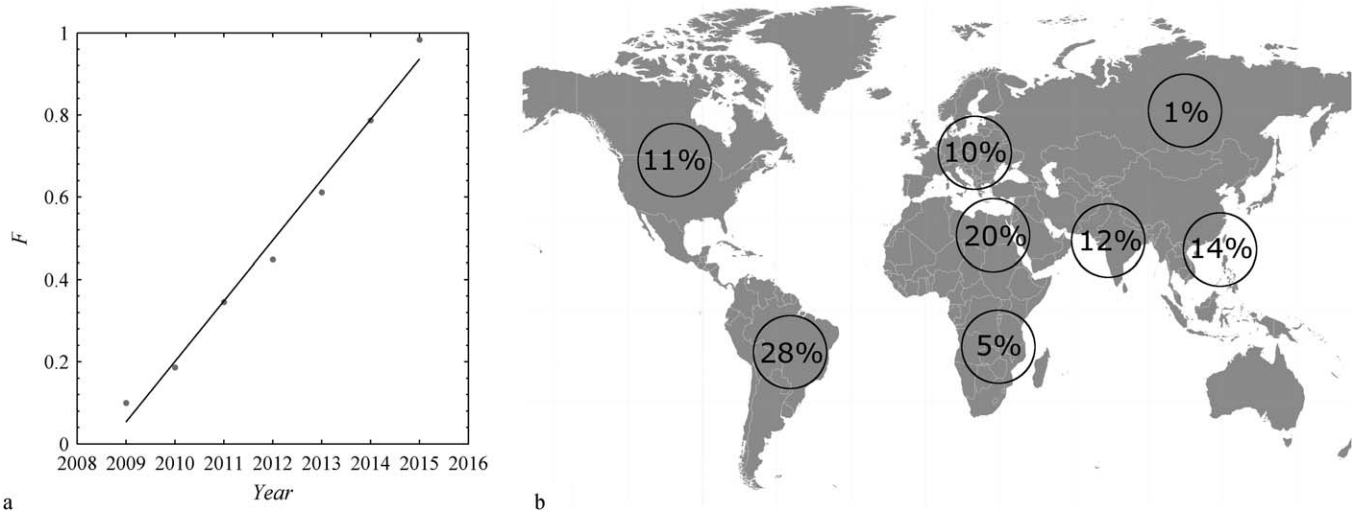

Figure 1. (a) Cumulative relative frequency *F* of the retrieved footages by year of publication, and (b) spatial distribution of the retrieved videos documenting human stability/instability in a flow.

The research provided 311 videos but only 98 of them (see supporting information Appendix A) allowed proper quantification of local flow depth and velocity. Considering that several footages permitted the evaluation of more than a single stability case, eventually 125 different events involving children (2.4%), teenagers (2.4%), and adults (95.2%) were studied.

3. Methods

3.1. Measurements of Water Elevation and Velocity

The stability of individuals under the action of flow is usually evaluated as a function of flow depth and velocity, with the possible influence of local slope and liquid density [e.g., *Milanesi et al.*, 2015]. This section describes the techniques used to compute flow depth and velocity in the selected footages.

First, a physical linear scaling length S_r (m), corresponding to a screen scaling length S_s (su, "screen unit" in the following) measured in graphical units on the screen, must be identified. Then the physical length of interest L_r (m) can be calculated from the corresponding screen length L_s (su) as:

$$L_r = \frac{S_r}{S_s} L_s \tag{1}$$

In some cases, the person impacted by the flow is close to objects of known size (e.g., vehicles of known make and model and persons whose identity is known) that could provide the physical scaling length S_r (m). Alternatively, S_r (Figure 3) could be calculated by measuring in screen units different body segments of the subject. It is important to stress that the actual values of height and body segments length of the impacted subject are usually unknown. However, it is possible to obtain the average height of the population Y_{avg} (m) of the region where the video was recorded and the length of each body segment from literature studies based on robust statistical analyses [e.g., *Gordon et al.*, 1989]. Accordingly, as shown in the following, the final results are computed on the basis of these average values with uncertainty bounds accounting for the intrinsic variability of the body sizes.

Figure 2. Examples of (a) low-resolution image (source: https://www.youtube.com/watch?v=LqvNS0Wwx9c) and (b) footage recorded from high position (source: https://www.youtube.com/watch?v=66lFAvJM3Vc).

Once the scaling length is identified for each situation, the flow depth h (m) and velocity U (m s^{-1}) can be calculated. Usually, only the unsubmerged part of the

Figure 3. Example of identification of the scaling length. In this case, the outer sleeve seam length (blue line), that according to *Gordon et al.* [1989] is on average 34.3% of the total height, was used to estimate the unsubmerged body height (green line). The run-up height was calculated on a different frame (source: https://www.youtube.com/watch?v=hut-r1TVyho).

impacted body can be observed. Accordingly, it can be subtracted from the average height of people Y_{avg} of the same sex and age in the considered geographic area in order to calculate the flow depth.

Flow velocity can be computed by measuring the travel time of floating bodies between two points at known distance. This procedure provides an estimate of the surface flow velocity that, assuming a power law velocity profile, is about 16% greater than the average velocity.

The vertically averaged velocity U_∞ upstream of the obstacle, where the flow depth is h_∞, can be computed by the Bernoulli's equation. For this calculation, the flow of an inviscid, incompressible fluid around a vertical cylinder can be considered. At the leading edge of the cylinder, a stagnation point is formed where the oncoming flow is brought to rest.

The pressure distribution on the upstream side of the cylinder is very well represented by the solution of Laplace's equation as far as 30° from forward stagnation point for a wide range of Reynolds number of the cylinder (Figure 4a). The same solution provides the dimensionless conversion η of kinetic to potential energy head as:

$$\eta \equiv \frac{h-h_\infty}{\frac{U_\infty{}^2}{2g}} = \frac{2x^2-2y^2-1}{(x^2+y^2)^2} \tag{2}$$

where $x = X/R$ and $y = Y/R$ are dimensionless space coordinates, R (m) is the cylinder radius, and h is the flow depth at point (x,y). At the stagnation point ($x = -1$, $y = 0$), equation (2) leads to:

$$\frac{U_\infty{}^2}{2g} = h-h_\infty \tag{3}$$

which can be used to calculate the mean velocity upstream of the cylinder:

$$U_\infty = \sqrt{2g(h-h_\infty)} \tag{4}$$

This reasoning is especially true as long as the incoming flow is subcritical so that no significant energy dissipation occurs in front of the object. At the same time, in the field of velocity $U < 1$ m s^{-1}, the water rise would be lower than 0.05 m, so that it could be difficult to measure. Accordingly, this field would be better modeled with the floating body method. In case of supercritical currents, equation (4) is partly violated because the run-up has a stronger level of turbulence and the specific energy of the undisturbed flow might be higher than the one provided by the run-up. Accordingly, in this case, equation (4) might underestimate the actual U_∞, providing a conservative evaluation of the stability threshold. This approach can be applied to individuals in a flow (Figure 4b) by substituting $h = h_2$ and $h_\infty = h_1$ in equation (4). For this purpose, the subject impacted by the flow must have negligible relative movement with respect to the flow.

In cases of supercritical currents, the flow velocity might also be related to the angle of the wake downstream of the impacted body. Finally, when the geometric configuration suggests a transition of a mild flow through the critical depth, the velocity can be computed by measuring the flow depth in correspondence to the drop.

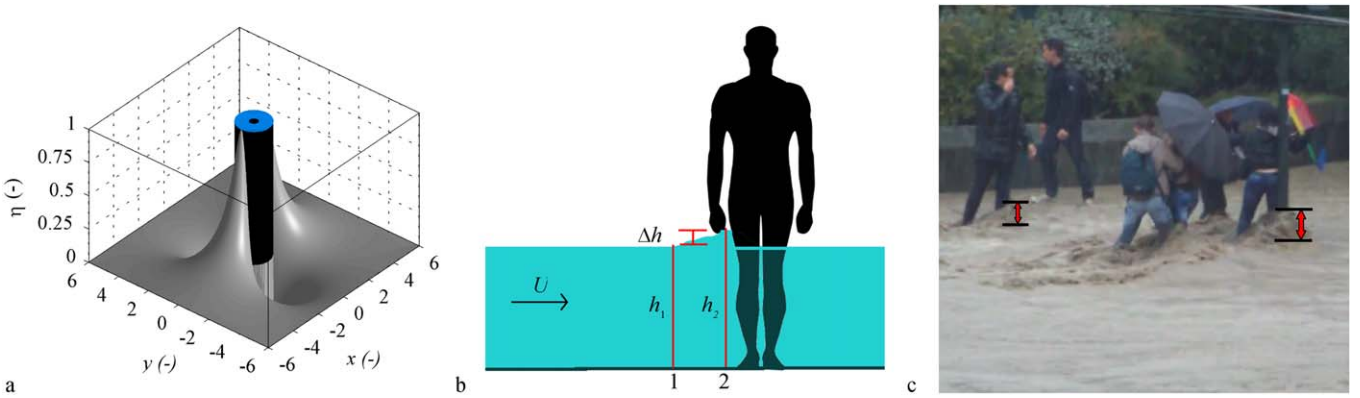

Figure 4. (a) Flow field of an inviscid fluid around a cylinder. (b) Scheme of application of the Bernoulli's equation to a person impacted by a flow, and (c) visualization of the run-up height shown by the red arrows (source: https://www.youtube.com/watch?v=DizsJcjLuOM).

3.2. Quantification of Uncertainty and Validation

The computed data were derived from images taken with different focal lengths and different visual angles. In this study, the scaling length was usually observed for the same person for which the flow depth was measured and only videos shot with low zenithal angles (measured from the horizontal direction) were selected. Accordingly, due to the close proximity of the scaling length and the measured quantity of interest, the problem of image distortion appears negligible. In order to validate these assumptions, a graduated ruler was photographed in correspondence to different focal lengths (18, 35, and 55 mm; APS-C camera), zenithal angles (up to 45°), and distances (up to 7 times the ruler length). The ruler length was then estimated with equation (1), using a known fraction (20%) of the ruler as the scaling length. A maximum error of 6% between real and computed ruler length was observed when the zenithal shooting angle is 45°. For angles below 30° the error is lower than 4% and it reduces for increasing distances between the camera and the ruler. No independent relevant effects of the focal length were observed.

Under the hypothesis that the operator is sufficiently well trained and no error is introduced through image processing, the uncertainty of the computed flow depths and velocities is mostly related to the intrinsic variability of the body features described by the statistics of the population height and of the length of the body segments [e.g., *Gordon et al.*, 1989]. The uncertainty was computed by a direct method for error propagation accounting for the dispersion of these parameters around their mean value. The uncertainty E of a combination f of the measured quantities x_i can be written as:

$$E = \sum \left| \frac{\partial f}{\partial x_i} \right| \Delta x_i \tag{5}$$

where Δx_i is the uncertainty associated with each variable. The population of heights and lengths of the body segments are reasonably well represented by a truncated normal distribution. Under the hypothesis that they are independent and their ratio is normally distributed, the uncertainty Δx_i including 95% of the total population can be calculated as $2\sigma_{xi}$, where σ is the standard deviation.

The methodology proposed to compute the flow depth was validated by comparing the computed depth h_c (m) obtained from six videos with scaling lengths of known size (the dimension of vehicles or the height of a subject of known identity) with the results h_s (m) and the associated uncertainties calculated through the statistical anthropometric studies [*Gordon et al.*, 1989]. This comparison (Figure 5a) showed that all the points computed on the basis of known quantities are contained within the calculated uncertainty bounds of the statistical values:

$$h_s - E(h_s) < \; h_c \; < \; h_s + E(h_s) \tag{6}$$

where $E(h_s)$ is the uncertainty associated with h_s. This procedure was also tested on 20 Italian subjects equipped with a level staff and photographed at a distance of about 10 m and a zenithal angle of 0°. Three different focal lengths (18, 35, and 55 mm; APS-C camera) were tested. For each subject and each focal length, three different ideal flow depths were observed on the staff (0.3, 0.6, and 0.9 m) and compared with

Figure 5. (a) Comparison between flow depths calculated using known scaling length (h_c) and the statistical approach (h_s). (b, c) Experimental tests performed by *Jonkman and Penning-Rowsell* [2008] and *Martínez-Gomariz et al*. [2016] with indication of the quantities used to calculate flow depth and velocity: unsubmerged height (green), run-up height (red), and scaling length (blue). (modified from *Jonkman and Penning-Rowsell* [2008] and *Martínez-Gomariz et al*. [2016]).

the values estimated using a scaling length of the shoulder-elbow length (equation (1)). Ninety-five percent of the performed tests fulfilled the previously mentioned condition. These tests did not show any influence of the focal length.

Laboratory tests were conducted to validate the procedure for the computation of flow velocity with equation (4). The experiments were set up for a rectangular cross-section flume with a discharge of 0.004 $m^3\ s^{-1}$ measured by an electromagnetic flow meter. A graduated circular cylinder of diameter 0.02 m was placed in the current to calculate the run-up height as the difference between the flow depth in correspondence with the upstream side of the obstacle and the flow depth in the absence of the cylinder. The undisturbed averaged flow velocity was calculated as the ratio between the discharge and the cross-sectional area. In the subcritical flow test, the measured velocity was 0.28 ± 0.004 m s^{-1} instead of 0.30 ± 0.070 m s^{-1} calculated by equation (4). In the supercritical flow test, the measured velocity was 0.84 ± 0.022 m s^{-1} instead of 0.78 ± 0.053 m s^{-1} calculated by equation (4). In both cases, the difference of the mean values is about 8% and is within the error bound of the estimates.

Finally, the proposed procedure was tested against pictures or videos from experimental tests documented in the literature. The obtained results were compared with the measured data from *Jonkman and Penning-Rowsell* [2008] (Table 1, footnote b) regarding a professional stuntman standing in a real channel flow (Figure 5b) and from *Martínez-Gomariz et al*. [2016] (Table 1, footnote c) showing a Spanish woman impacted by the current (Figure 5c). In both cases, the reliability of the overall procedure is confirmed since the measured quantities (U_c,h_c) are contained in the intervals defined by the computed statistical values (U_s,h_s) bounded by the related uncertainties.

4. Results and Discussion

The proposed approach provided 125 (*U,h)* values, mostly characterized by $h < 0.7$ m, that is often considered a reference threshold also for buildings vulnerability [e.g., *Fuchs et al*., 2007]. This distribution reflects the trivial observation that people only reluctantly attempt to cross deep, dangerous looking currents. The size of this data set will increase with time and it complements the literature experimental data, mostly limited to $h < 1$ m and never higher than $h \approx 1.2$ m.

Each point of the presented data set was classified according to three different situations, on the basis of the behavior of the subject (see Table 2 and Figure 6). The condition is "stable" when the person impacted by the flow confidently stands in the water. "Instability" occurs when the person loses control of his/her posture and is swept away by the flow. Finally, there are some situations where a person strives to maintain equilibrium by adjusting his/her posture, in a situation of "incipient instability." For convenience, these cases

Table 1. Summary of the Complete Validation Tests Based on Literature Data

Subject	Y_{avg} (m)	σ (Y_{avg}) (m)	S_s (su)	S_r[a] (m)	Y_{avg}-h (su)	h_2-h_1 (su)	h_s (m)	U_s (m s^{-1})	h_c (m)	U_c (m s^{-1})
1[b]	1.753	0.089	9.44	0.37	36.31	7.92	0.34 ± 0.12	2.46 ± 0.20	0.35	$2.4 \div 2.6$
2[c]	1.662	0.062	468.45	0.35	2111.46	331.54	0.12 ± 0.11	2.18 ± 0.15	0.15	2.15

[a]Calculated by considering the shoulder elbow length, i.e., $0.21 \cdot Y_{avg}$ [*Gordon et al*.,1989].
[b]Adult English male tested by *Jonkman and Penning-Rowsell* [2008] ($m = 68.25$ kg; $Y = 1.70$ m). Y_{avg} and $\sigma(Y_{avg})$ from Moody [2013].
[c]Adult Spanish female tested by *Martínez-Gomariz et al*. [2016] ($m = 56$ kg; $Y = 1.59$ m). Y_{avg} and $\sigma(Y_{avg})$ from *Garcia and Quintana-Domeque* [2007].

can be placed at the boundary between stability and instability and, in the following, will be classified as "incipient instability."

In Figure 6, stable and unstable points are represented with green and red markers, respectively, and three partly overlying regions can be observed. The "incipient instability" data (represented by blue markers in Figure 6) are reasonably centered on the stability thresholds calculated for adults by both *Milanesi et al*. [2015] and *Xia et al*. [2014].

Yee [2003] and *Foster and Cox* [1973] investigated the "incipient instability" for children and teenagers (Figure 6c) providing a lower envelope for the instability data calculated from the videos. A wider set of experimental literature data is available for adults (Figure 6d). The points by *Jonkman and Penning-Rowsell* [2008] are in good agreement with some "incipient instability" points extrapolated from the videos. The data by *Russo et al*. [2013] and *Martínez-Gomariz et al*. [2016], measured with the same experimental setup, should be considered an extreme lower bound of adults' instability in a flow, due to the effect of bed slope, unsuitable shoes, and bad lighting conditions. Similarly, the data by *Takahashi et al*. [1992] were measured testing small subjects and, accordingly, low (U,h) values. The experimental points by *Karvonen et al*. [2000] are in good agreement with the data computed in this study and the upper envelope of their experimental points limits the set of the "stability" points computed here. In a real flood situation, *Chanson and Brown* [2015] experienced velocity and depth turbulent fluctuations with variations up to ± 0.5 m s^{-1} and ± 0.15 m, respectively. Accordingly, they suggested that the threshold conditions should be represented as an area on the U-h plane. In this study, the average extent of the uncertainty bounds computed from the videos on the basis of the 2σ range, is ± 0.092 m for flow depth and ± 0.118 m s^{-1} for velocity (Figure 7).

The observed scattering of the experimental and measured data indicates the inherently stochastic nature of the problem. Accordingly, in order to obtain a statistically significant stability surface, the following method is proposed. As a first observation, considering that human instability is a monotonically increasing function of U and h, each "incipient instability" couple $(\bar{U}, \bar{h})$ subdivides the U-h space into two subregions: an upper region of "instability" (red shaded area in Figure 8a) characterized by an unitary vulnerability coefficient and a lower "stability" one (blue shaded area in Figure 8a) with a zero vulnerability coefficient. In order to take into account the uncertainty of each couple $(\bar{U}, \bar{h})$, quantified by its uncertainty, a $\pm E$ (see equation (5)) rectangular neighborhood of $(\bar{U}, \bar{h})$ should be considered. Accordingly, eight additional different possibilities (from A_1 to A_8) were taken into account by changing $\pm E$ for one (A_1, A_2, A_3, and A_4) or both (A_5, A_6, A_7, and A_8) of the independent variables. A probability was associated with each case: p_0 was assigned to the A region identified by the couple $(\bar{U}, \bar{h})$, p_1 to the four cases from A_1 to A_4, p_2 to the cases from A_5 to A_8, with the constraint $p_0 + 4(p_1 + p_2) = 1$. Under the assumption of a bivariate normal distribution of two independent variables, the following values were used: $p_0 = 0.46$, $p_1 = 0.1135$, and $p_2 = 0.0215$. An elementary vulnerability surface $v_i(U,h)$ can finally be associated with the couple $(\bar{U}, \bar{h})$ as a probability weighted average of the nine cases from A to A_8. The same type of subdivision and weighted average can be applied to stability (Figure 8b) and instability data (Figure 8c). In the first case, only the stability region is associated

Table 2. Number of Situations in Each Category and Percent Over the Total Amount

	All Videos	Children	Teenagers	Adults
Stability	97 (77.6%)	1 (0.8%)	1 (0.8%)	95 (76.0%)
Incipient instability	14 (11.2%)		1 (0.8%)	13 (10.4%)
Instability	14 (11.2%)	2 (1.6%)	1 (0.8%)	11 (8.8%)
TOTAL	125	3 (2.4%)	3 (2.4%)	119 (95.2%)

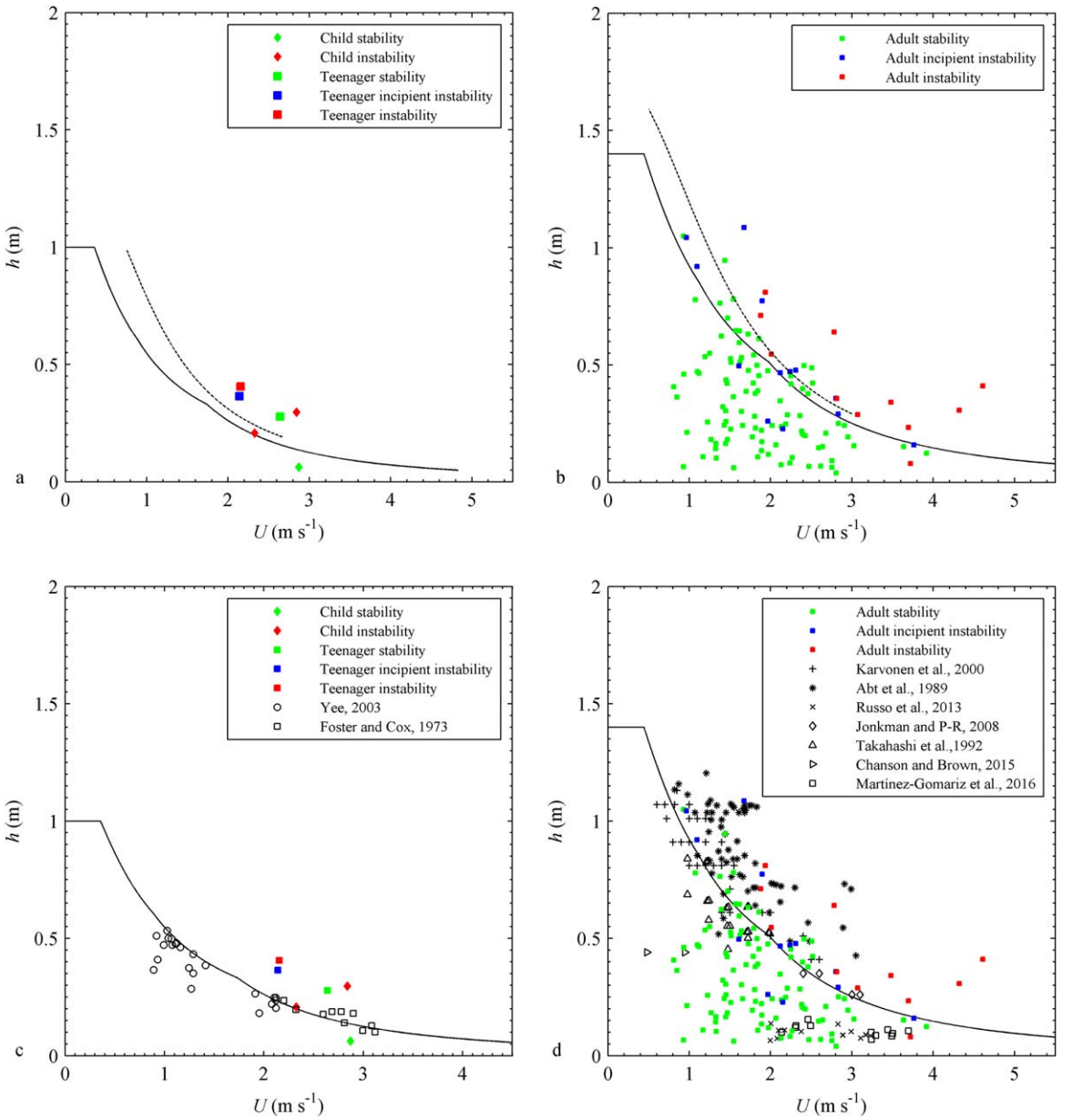

Figure 6. Points extrapolated from the selected videos and conceptual stability thresholds for (a) children and (b) adults proposed by *Milanesi et al.* [2015] and *Xia et al.* [2014] in continuous and dashed lines, respectively. Comparison of the points of (b) children, (c) teenagers, and (d) adults with the literature experimental data and with the conceptual model of *Milanesi et al.* [2015].

with the couple $(\bar{U}, \bar{h})$ because it is not possible to identify an instability region on the *U-h* space. Similarly, in the second case, only the instability region can be identified with no definite information on the related stability region.

Although "incipient instability" conditions are the most informative ones, also $(\bar{U}, \bar{h})$ stable and unstable points were used to identify vulnerability surfaces $v_i(U,h)$ that limit from below and from above the transition area of the final vulnerability surface $V(U,h)$. Finally, this surface can be computed by averaging the elementary vulnerability surfaces $v_i(U,h)$ from the N available points:

$$V(U,h) = \frac{\sum_{i=1}^{N} v_i(U,h)}{N} \tag{7}$$

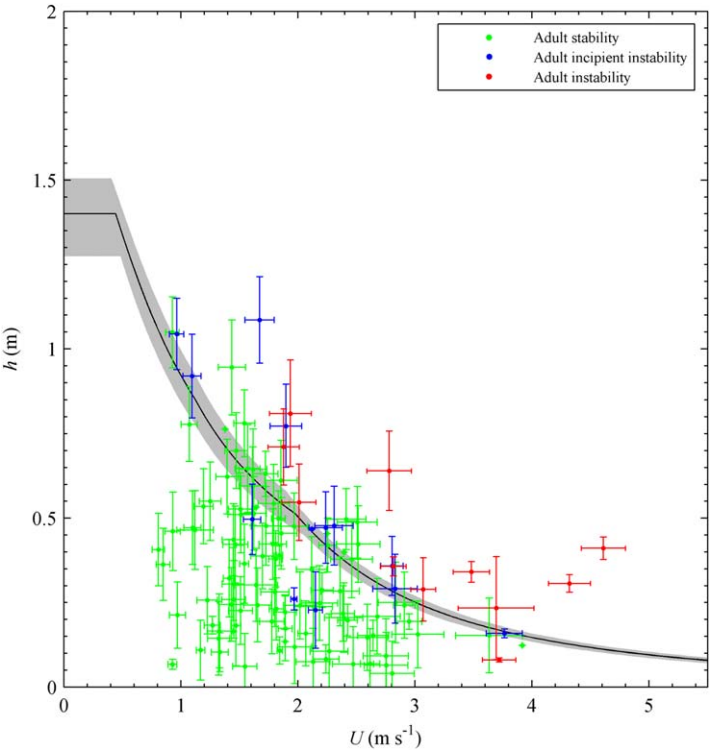

Figure 7. Uncertainty bounds of the extrapolated points and comparison with the conceptual threshold by *Milanesi et al.* [2015]. The shaded area accounts for the variability of the stability curve of adults with height ranging between 1.57 and 1.85 m and mass between 58 and 85 kg.

The $V(U,h)$ surface provides a probabilistic description of the stability data and can be used to define stability thresholds on the U-h plane associated with predetermined percentile values, to be used in risk zoning. The proposed approach was applied to the data composed of the computed points from the selected footages and complemented with the literature experimental values. Whereas the estimated uncertainty was used for the video data set, the relative instrumental errors estimated by *Jonkman and Penning-Rowsell* [2008] for their experimental data was used to compute the uncertainty of other literature laboratory data. The resulting surface is shown in Figure 9a. The theoretical curve for an adult [*Milanesi et al.*, 2015] closely approximates the 50th percentile curve in a wide range of U and h (Figure 9b).

The irregular pattern of the surface in Figure 9a is a consequence of the limited number of data in the sample. However, the growing available information will lead to a larger data set. Accordingly, we can expect that the computed surface will asymptotically converge to the "real" stability surface (Figure 10c). To simulate this process, the described procedure was applied to a synthetically computed sample obtained by adding a stochastic component to the threshold velocity of the deterministic curve by *Milanesi et al.* [2015]. Three samples with 350, 2000, and 20,000 data where randomly generated and the corresponding surfaces computed (Figure 10).

5. Conclusions

Flood vulnerability models describe the expected damage suffered by different categories of exposed targets and are fundamental tools in a rational framework for quantitative risk assessment. Both empirical and conceptual models are available and their calibration is based on experimental data. Limiting the attention to people's vulnerability to floods, all the available literature data were derived either under controlled conditions, where people's stability was tested in laboratory flumes, or real channel, or through scaled models. In spite of the high quality of the measurements, the data are beset by two major defects. First, they are limited in number and require expensive experiments. Second, there is evidence that they do not properly represent real hazard situations, when a wide range of untrained people in different environmental conditions must cope with unexpected events. As a matter of fact, stability is conditioned by several environmental, individual, and psychological factors. Although detailed laboratory studies can carefully measure the primary physical variables that control the stability of a person, they cannot replicate the overall context of a flood situation and cannot represent the intrinsic variability that could be observed by testing a multitude of subjects.

This paper suggests an approach based on citizen science to overcome these limitations, complementing laboratory data, and increasing the overall availability of data on human vulnerability. This study introduced the use of information derived from footages available on the web regarding accidents of people impacted

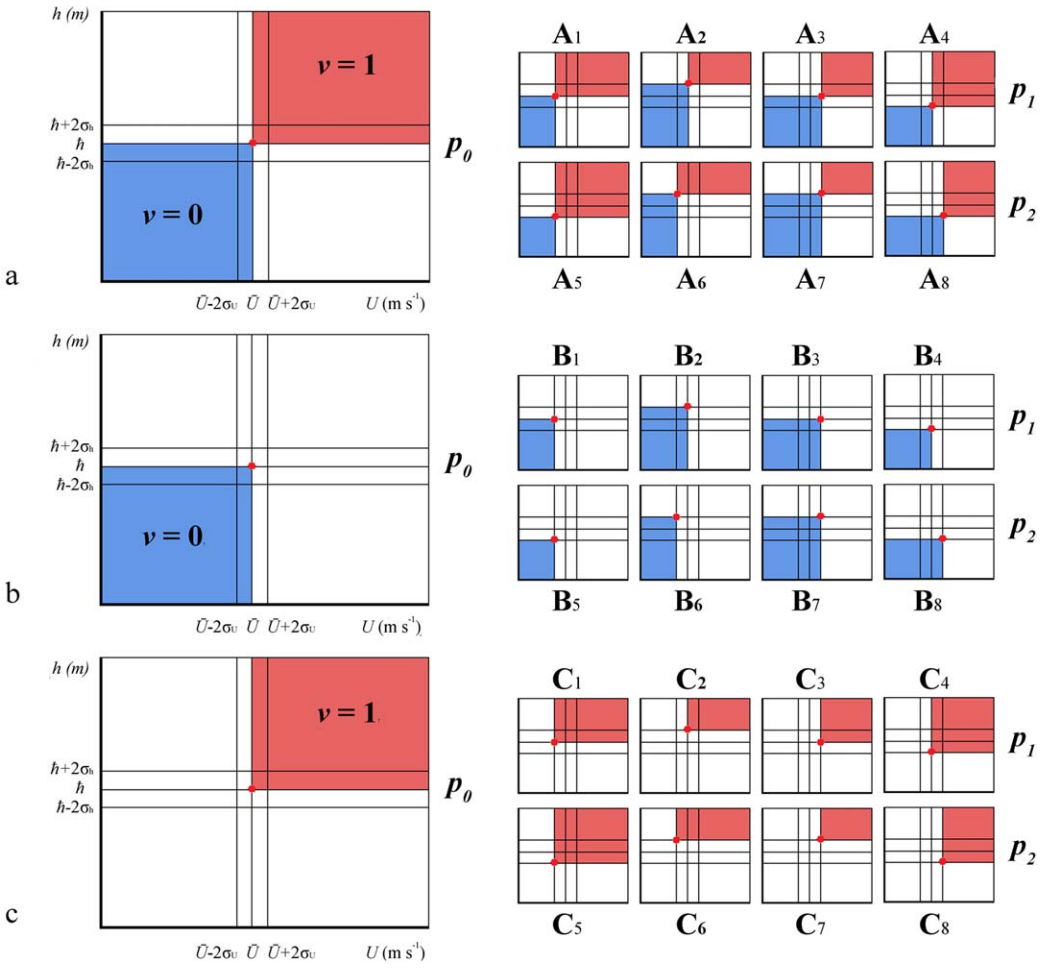

Figure 8. (a) Representation of the *U-h* space partition exerted by a $(\bar{U}, \bar{h})$ couple corresponding to an incipient instability condition that separates stability (blue) and instability (red) regions. The partitions from A_1 to A_8 are defined on the basis of the uncertainty bounds of the $(\bar{U}, \bar{h})$ couple. The partitions associated with $(\bar{U}, \bar{h})$ (b) stability or (c) instability situations.

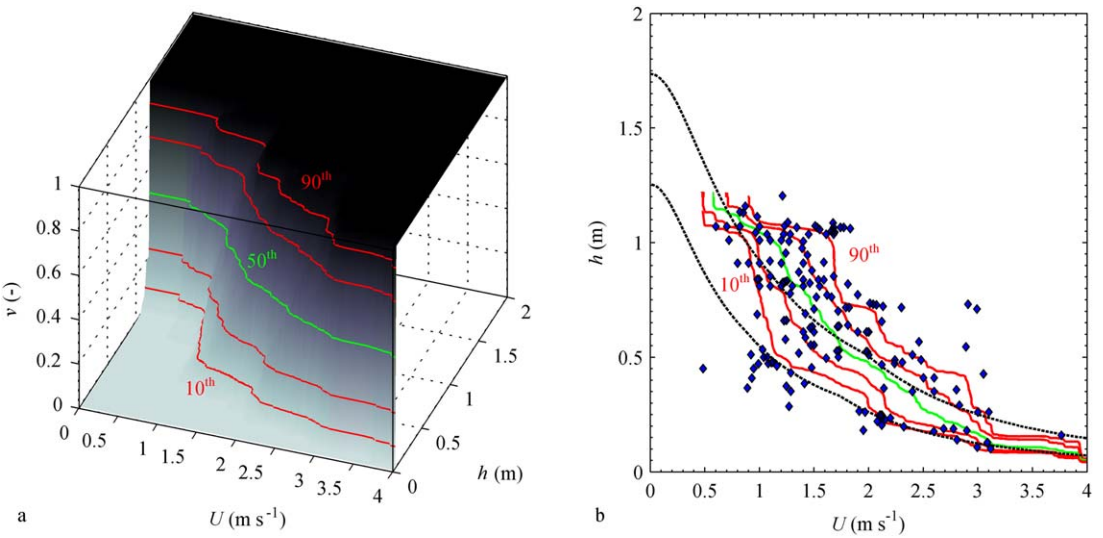

Figure 9. Surface of human instability (a) computed using literature experimental data and the points computed from the videos (blue dots in Figure 9b). (b) The contours corresponding to the 10th, 25th, 50th, 75th, and 90th percentile. The dotted lines correspond to the incipient instability curve for adults (upper curve) and children (lower curve) suggested by *Milanesi et al.* [2015].

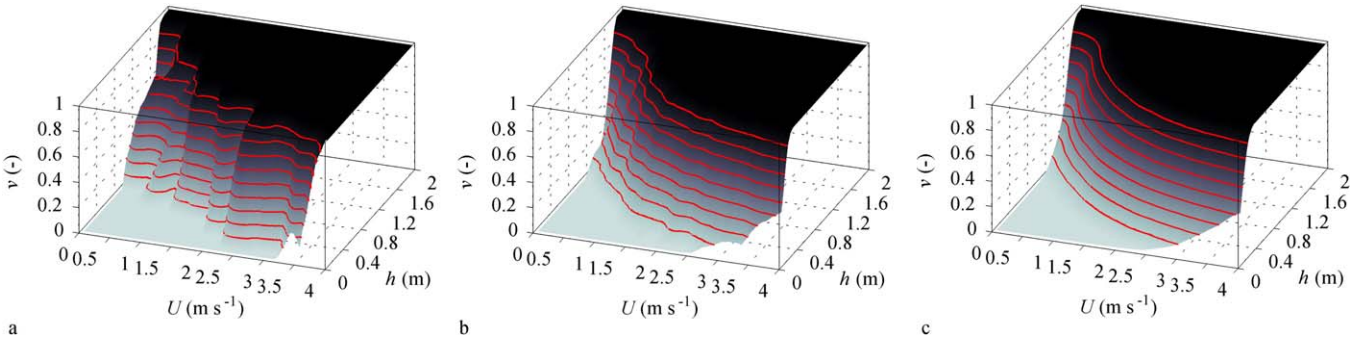

Figure 10. Example of convergence to the asymptotic probability distribution of human instability in a flow represented on the *U-h* plane. Surfaces (a), (b), and (c) were generated by using 350, 2000, and 20,000 data, respectively. Black areas correspond to total instability and the grey areas indicate complete stability. The red iso-percentile lines represent instability threshold curves.

by a flow. Flow depth and velocity were calculated by measuring geometric quantities on the frames and were related to the conditions of stability of the involved subjects. The proposed statistical procedure is affected by larger uncertainties than experimental data. However, the amount of real information that can be retrieved by this approach will provide a statistically significant data set, where single measurement errors will asymptotically compensate each other, converging to a real surface of people's vulnerability to floods. Accordingly, the data set in supporting information Appendix A should be regarded as the starting point of a self-sustaining process to increase the available information to reach this goal.

Acknowledgments

We wish to acknowledge H. Chanson for the interesting and fruitful exchange of ideas occurred during the preparation of the paper. We would also thank S. N. Jonkman and E. Martínez-Gomariz for the permission of use of the images from their laboratory activities. The contribution of A. Mazzino is kindly acknowledged. Finally, we are grateful to the Editor and the Reviewers for their valuable suggestions on the improvement of the paper quality. We acknowledge the help of S. Chapra (Tufts University) for his revision of the final manuscript. The literature data used in this study can be accessed in the cited papers. Supporting information Appendix A containing the data computed from the videos can be downloaded from: http://hydraulics.unibs.it/hydraulics/?page_id=2904. This work has been funded by the Flagship Project RITMARE—The Italian Research for the Sea—coordinated by the Italian National Research Council and funded by the Italian Ministry of Education.

References

Abt, S. R., R. J. Wittler, A. Taylor, and D. J. Love (1989), Human stability in high flood hazard zone, *Water Resour. Bull.*, *25*(4), 881–890, doi:10.1111/j.1752-1688.1989.tb05404.x.

Adhikari, P., Y. Hong, K. R. Douglas, D. B. Kirschbaum, J. Gourley, R. Adler, and G. R. Brakenridge (2010), A digitized global flood inventory (1998–2008): Compilation and preliminary results, *Nat. Hazards*, *55*(2), 405–422, doi:10.1007/s11069-010-9537-2.

Aureli F., S. Dazzi, A. Maranzoni, P. Mignosa and R. Vacondio (2015), Experimental and numerical evaluation of the force due to the impact of a dam-break wave on a structure, *Adv. Water Resour.*, *76*, 29–42, doi:10.1016/j.advwatres.2014.11.009.

Barredo, J. I. (2009), Normalised flood losses in Europe: 1970–2006, *Nat. Hazards Earth Syst. Sci.*, *9*(1), 97–104, doi:10.5194/nhess-9-97-2009.

Becker, J. S., H. L. Taylor, B. J. Doody, and K. C. Wright (2015), A review of people's behavior in and around floodwater, *Weather Clim. Soc.*, *7*(4), 321–332.

Buytaert, W., A. Dewulf, B. De Bièvre, J. Clark, and D. M. Hannah (2016), Citizen science for water resources management: Toward polycentric monitoring and governance?, *J. Water Resour. Plann. Manage.*, *142*(4), 1–4, doi:10.1061/(ASCE)WR.1943-5452.0000641.

Chanson, H., and R. Brown (2015), Discussion on: New criterion for the stability of a human body in floodwaters. By J. Xia, R. A. Falconer, Y. Wang and X. Xiao, *J. Hydraul. Res.*, *53*(4), 540–541, doi:10.1080/00221686.2015.1054321.

Cohn, J. P. (2008), Citizen science: Can volunteers do real research?, *BioScience*, *58*(3), 192–197, doi:10.1641/B580303.

Costabile P., C. Costanzo and F. Macchione (2016), Performances and limitations of the diffusive approximation of the 2-d shallow water equations for flood simulation in urban and rural areas, *Appl. Numer. Math.*, doi:10.1016/j.apnum.2016.07.00, in press.

Cox, R. J., T. D. Shand, and M. J. Blacka (2010), *Australian Rainfall and Runoff Revision Project 10: Appropriate Safety Criteria for People*, Eng. Aust., Barton, Australia.

Cross, R. (1967), Tsunami surge forces, *J. Waterw. Harbors Div.*, *93*(4), 201–231.

Dickinson, J. L., J. Shirk, D. Bonter, R. Bonney, R. L. Crain, J. Martin, T. Phillips, and K. Purcell (2012), The current state of citizen science as a tool for ecological research and public engagement, *Frontiers Ecol. Environ.*, *10*(6), 291–297, doi:10.1890/110236.

Foster, D. N., and R. Cox (1973), Stability of children on roads used as floodways, *Tech. Rep. 13/73*, Univ. of N. S. W., Water Res. Lab., Sidney, Australia.

Fuchs, S., K. Heiss, and J. Hübl (2007), Towards an empirical vulnerability function for use in debris flow risk assessment, *Nat. Hazards Earth Syst. Sci.*, *7*(5), 495–506, doi:10.5194/nhess-7-495-2007.

Fuchs, S., M. Keiler, and A. Zischg (2015), A spatiotemporal multi-hazard exposure assessment based on property data, *Nat. Hazards Earth Syst. Sci.*, *15*(9), 2127–2142, doi:10.5194/nhess-15-2127-2015.

Garcia, J., and C. Quintana-Domeque (2007), The evolution of adult height in Europe: A brief note, *Econ. Human Biol.*, *5*(2), 340–349, doi:10.1016/j.ehb.2007.02.002.

Gordon, C. C., T. Churchill, C. E. Clauser, B. Bradtmiller, J. T. McConville, I. Tebbetts, and R. A. Walker (1989), Anthropometric survey of US Army personnel: Summary statistics, interim report for 1988, report NATICK/TR-89/044, Anthropol. Res. Project Inc., Yellow Springs, Ohio.

Güneralp, B., I. Güneralp, and Y. Liu (2015), Changing global patterns of urban exposure to flood and drought hazards, *Global Environ. Change*, *31*, 217–225, doi:10.1016/j.gloenvcha.2015.01.002.

Ishigaki, T., Y. Onishi, Y. Asai, K. Toda, and H. Shimada (2008), *Evacuation criteria during urban flooding in underground space, paper presented at 11th ICUD*, IAHR/IWA, Edinburgh, U. K.

Jongman, B., E. E. Koks, T. G. Husbyand, and P. J. Ward (2014), Increasing flood exposure in the Netherlands: Implications for risk financing, *Nat. Hazards Earth Syst. Sci.*, *14*(5), 1245–1255, doi:10.5194/nhess-14-1245-2014.

Jonkman, S. N., and E. Penning-Rowsell (2008), Human instability in flood flows, *J. Am. Water Resour. Assoc.*, *44*(5), 1208–1218, doi:10.1111/j.1752-1688.2008.00217.x.
Karvonen, R. A., H. K. Hepojoki, H. K. Huhta, and A. Louhio (2000), The use of physical models in dam-break flood analysis, Development of Rescue Actions Based on Dam-Break Flood Analysis (RESCDAM), final report, Helsinki Univ. of Technol., Finnish Environ. Inst., Helsinki.
Keller, R. J., and B. Mitsch (1993), Safety aspects of the design of roadways as floodways, *Res. Rep. 69*, Urban Water Res. Assoc. of Aust., Melbourne, Australia.
Kundzewicz, Z. W., et al. (2014), Flood risk and climate change: Global and regional perspectives, *Hydrol. Sci. J.*, *59*(1), 1–28, doi:10.1080/02626667.2013.857411.
Lind, N., D. Harftord, and H. Assaf (2004), Hydrodynamic models of human stability in a flood, *J. Am. Water Resour. Assoc.*, *40*(1), 89–96, doi:10.1111/j.1752-1688.2004.tb01012.x.
Love, D. J. (1987), Analysis of a high hazard flood hazard zone, technical report, City of Boulder, Boulder, Colo.
Martínez-Gomariz, E., M. Gómez, and B. Russo (2016), Experimental study of the stability of pedestrians exposed to urban pluvial flooding, *Nat. Hazards*, *82*, 1259–1278, doi:10.1007/s11069-016-2242-z.
Maurais, J. (2003), Towards a new linguistic world order?, in *Languages in a Globalising World*, edited by J. Maurais and M. A. Morris, pp. 13–36, Cambridge Univ. Press, Cambridge, U. K.
Mazzoleni, M., L. Alfonso, J. Chacon-Hurtado, and D. Solomatine (2015), Assimilating uncertain, dynamic and intermittent streamflow observations in hydrological models, *Adv. Water Resour.*, *83*, 323–339, doi:10.1016/j.advwatres.2015.07.004.
Merz, B., H. Kreibich, R. Schwarze, and A. Thieken (2010), Review article "Assessment of economic flood damage", *Nat. Hazards Earth Syst. Sci.*, *10*(8), 1697–1724, doi:10.5194/nhess-10-1697-2010.
Meyer, V., et al. (2012), Recommendations for the user-specific enhancement of flood maps, *Nat. Hazards Earth Syst. Sci.*, *12*(5), 1701–1716, doi:10.5194/nhess-12-1701-2012.
Milanesi, L., M. Pilotti, and R. Ranzi (2015), A conceptual model of people's vulnerability to floods, *Water Resour. Res.*, *51*(1), 182–197, doi:10.1002/2014WR016172.
Min, S. K., X. Zhang, F. W. Zwiers, and G. C. Hegerl (2011), Human contribution to more intense precipitation extremes, *Nature*, *470*, 378–381, doi:10.1038/nature09763.
Montanari, A., G. Blöschl, X. Cai, D. S. Mackay, A. M. Michalak, H. Rajaram, and G. Sander (2013), Editorial: Toward 50 years of Water Resources Research, *Water Resour. Res.*, *49*, 7841–7842, doi:10.1002/2013WR014986.
Moody, A. (2013), *Adult Anthropometric Measures, Overweight and Obesity, Health Survey for England–2012*, Health and Soc. Care Inf. Cent., Leeds, U. K.
Muis, S., B. Güneralp, B. Jongman, J. C. Aerts, and P. J. Ward (2015), Flood risk and adaptation strategies under climate change and urban expansion: A probabilistic analysis using Global data, *Sci. Total Environ.*, *538*, 445–457, doi:10.1016/j.scitotenv.2015.08.068.
Pan, D. Z., and H. Chanson (2015), Physical modelling of tidal bore dyke overtopping: implication on individual's safety, paper presented at 36th IAHR World Congress, Int. Assoc. for Hydro-Environ. Eng. and Res., The Hague, Netherlands.
Peduzzi, P., B. Chatenoux, H. Dao, A. De Bono, C. Herold, J. Kossin, F. Mouton, and O. Nordbeck (2012), Global trends in tropical cyclone risk, *Nat. Clim. Change*, *2*(4), 289–294, doi:10.1038/nclimate1410.
Pilotti, M., M. Tomirotti, G. Valerio, and B. Bacchi (2010), Simplified method for the characterization of the hydrograph following a sudden partial dam break, *J. Hydraul. Eng.*, *136*(10), 693–704, doi:10.1061/(ASCE)HY.1943-7900.0000231.
Pilotti, M., A. Maranzoni, M. Tomirotti, and G. Valerio (2011), The 1923 Gleno dam-break: Case study and numerical modelling, *J. Hydraul. Eng.*, *137*(4), 480–492, doi:10.1061/(ASCE)HY.1943-7900.0000327.
Pilotti, M., A. Maranzoni, L. Milanesi, M. Tomirotti, and G. Valerio (2014), Dam-break modeling in alpine valleys, *J. Mountain Sci.*, *11*(6), 1429–1441, doi:10.1007/s11629-014-3042-0.
Pilotti, M., L. Milanesi, and R. Ranzi (2016), People and buildings vulnerability to floods in mountain areas, paper presented at XIII INTERPRAEVENT Congress, INTERPRAEVENT, Lucerne, Switzerland, 30 May–2 June.
Russo, B., M. Gómez, and F. Macchione (2013), Pedestrian hazard criteria for flooded urban areas, *Nat. Hazards*, *69*(1), 251–265, doi:10.1007/s11069-013-0702-2.
Takahashi, S., K. Endoh, and Z.-I. Muro (1992), Experimental study on people's safety against overtopping waves on breakwaters, *Rep. 31(4)*, Port and Harbour Res. Inst., Yokosuka, Japan.
Totschnig, R., and S. Fuchs (2013), Mountain torrents: Quantifying vulnerability and assessing uncertainties, *Eng. Geol.*, *155*, 31–44, doi:10.1016/j.enggeo.2012.12.019.
Walder, J. S., P. Watts, and C. Waythomas (2006), Case study: Mapping tsunami hazard associated with debris flow into a Reservoir, *J. Hydraul. Eng.*, *132*(1), 1–11, doi:10.1061/(ASCE)0733-9429(2006)132:1(1).
Xia, J., R. A. Falconer, Y. Wang, and X. Xiao (2014), New criterion for the stability of a human body in floodwaters, *J. Hydraul. Res.*, *52*(1), 93–104, doi:10.1080/00221686.2013.875073.
Yee, M. (2003), Human stability in floodways, Undergraduate Honours thesis, Sch. of Civ. and Environ. Eng., Univ. of N. S. W., Sydney, Australia.